View metadata, citation and similar papers at core.ac.uk
brought to you by CORE
provided by Helsingin yliopiston digitaalinen arkisto

MATERIALS INTERFACES
www.advmatinterfaces.de

Highly Material Selective and Self-Aligned Photo-assisted Atomic Layer Deposition of Copper on Oxide Materials

Ville Miikkulainen, Marko Vehkamäki, Kenichiro Mizohata, Timo Hatanpää, and Mikko Ritala*

There is a growing need for bottom-up fabrication methods in microelectronic industry as top-down, lithography-based methods face increasing challenges. In Photo-assisted atomic layer deposition (Photo-ALD), photons supply energy to the deposition reactions on the surface. Here, a process and patterning for Photo-ALD of copper is reported, with inherently selective, self-aligned film growth without any photomasking or additive layers. Highly conductive and pure copper films are selectively deposited on tantalum oxide for over hundred nanometers of film thickness, while no copper deposits on silicon or aluminum oxide. On anatase titanium dioxide, copper deposition is crystal-facet selective. Selective deposition of a metal is realized on oxides, which has been especially challenging for ALD. This study indicates that the growth mechanism is closely related to photocatalysis: the photons interact with the material under the growing copper film, enabling the inherent selectivity. The findings provide promising material engineering schemes for microelectronics, photocatalysis, and photovoltaics.

1. Introduction

Self-limiting and irreversible gas-to-surface reactions are the descriptive features of atomic layer deposition (ALD).[1] The gaseous precursors in ALD react only with the surface, either through solely thermal reactions, or via plasma excitation step. The success of ALD in microelectronic applications is paved by the extreme conformality and uniformity, thickness control, and quality of ALD films, which are all enabled by the surface-controlled chemistry of the ALD processes. Film thickness is controlled at sub-nm level by number of ALD cycles. The lateral control over the film growth, that is, area-selective deposition (ASD), however, is much more challenging with ALD. Especially microelectronic applications call for ASD to meet the fabrication requirements as the critical feature dimensions shrink to nm level and patterning by top-down lithographic approaches becomes increasingly challenging.[2,3] Lithography masks need to be aligned at nm accuracy, which results inevitably to edge placement errors (EPE) upon even the slightest mask misalignments.

The conventional approaches to realize ASD in ALD can be classified into three main categories: 1) passivation of the non-growth areas; 2) activation of the growth areas; 3) use of inherently selective deposition chemistry. In category (1) the non-growth areas are functionalized with passivating self-assembled monolayers (SAM) or polymer films.[4,5] Typically selectivity loss takes place when precursors adsorb onto non-ideally assembled or partially degraded SAM. Precursor molecules adsorbed on SAM function as reactive sites for the following precursor doses and the selectivity is lost.[2] The passivation layer must also be completely removed prior to the next processing step. In category (2) the growth area surface is functionalized prior to ASD to enable the film growth.[6–7] The film then deposits only onto the functionalized surface leaving the other areas clean. This approach stipulates a clear contrast in the film nucleation on the non-growth and functionalized growth surfaces. It is thus mainly limited to metal ALD processes which nucleate much more readily on metal surfaces than on others. Furthermore, careful control of the dosing is required to sustain growth selectivity. Because the activation layer for ASD becomes buried by the ALD film, the next processing step can follow directly after. In category (3), the inherently selective ALD, the selectivity is ruled purely by the reactions between the precursors and surfaces of different materials on the substrate. On the surface of a thin film device structure being fabricated, different materials are exposed to the ALD precursors, but the film grows only onto certain preferred materials that thereby define the growth areas. This is genuinely bottom-up processing and reduces the overall patterning steps to their minimum. Since the patterns self-align, EPE is excluded. For these reasons, (3) is a very attractive option for ASD, but it is extremely challenging to control the surface chemistry to maintain ASD for several ALD cycles. Therefore (3) is mainly limited to ASD of metals.[8–9]

Dr. V. Miikkulainen, Dr. M. Vehkamäki, Dr. T. Hatanpää, Prof. M. Ritala
Department of Chemistry
University of Helsinki
P.O. BOX 55 (A.I. Virtasen aukio 1), Helsinki FI-00014, Finland
E-mail: ville.miikkulainen@aalto.fi

Dr. V. Miikkulainen
Department of Chemistry and Materials Science
Aalto University
Kemistintie 1, Espoo 02150, Finland

Dr. K. Mizohata
Department of Physics
P.O. Box 43 (Pietari Kalmin katu 2), Helsinki FI-00014, Finland

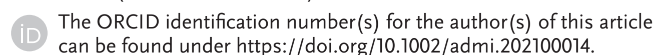
The ORCID identification number(s) for the author(s) of this article can be found under https://doi.org/10.1002/admi.202100014.

© 2021 The Authors. Advanced Materials Interfaces published by Wiley-VCH GmbH. This is an open access article under the terms of the Creative Commons Attribution License, which permits use, distribution and reproduction in any medium, provided the original work is properly cited.

DOI: 10.1002/admi.202100014

© 2021 The Authors. Advanced Materials Interfaces published by Wiley-VCH GmbH

Selective metal deposition on metals, by either chemical vapor deposition or ALD, is already a well-known concept.[9–10] Furthermore, selective semiconductor-on-semiconductor epitaxy has been in high-volume manufacturing for decades.[11] Besides the self-aligned deposition of materials, selective epitaxy is a very useful tool for strain engineering to tailor carrier mobility. In many cases, the selective metal-on-metal and semiconductor-on-semiconductor deposition processes can be controlled at a level that enables production. However, in semiconductor industry, there is urgent demand also for processes and approaches that would enable ASD of, for example, metals on dielectrics and metals on semiconductors. These approaches are critical for solving the future challenges in integration and device downscaling, such as self-aligned deposition of contacts and interconnects.

A much less studied approach for ASD is Photo-assisted ALD (Photo-ALD), where photons deliver energy to activate the deposition chemistry.[12–19] Photons excite either the adsorbed or gaseous precursors, or both, to facilitate ALD chemistry. ASD is straightforward for large features with Photo-ALD by simply masking the photon beam so that the non-growth areas are shadowed under the mask. With Photo-ALD, no pre- or post-treatments are needed to facilitate ASD, but the challenge with mask alignment and EPE remains. In our recent paper on Photo-ALD of metal oxides we report ASD but with a limited spatial resolution: the metal oxide film edge is not sharp but the film spreads also underneath the mask.[12] Even with an optimized mask design, the optical limits would be the bottleneck for the spatial resolution and the smallest obtainable feature size, which is not enough for the current nm-scale device-level patterning. Photo-ALD has been studied for deposition of only a limited number of materials, including GaAs, BN, and metal oxides.[12–19]

In the present study, we report Photo-ALD of copper films by employing copper dimethyl-aminopropanolate precursor and UV–Vis photons from a pulsed light source. The growth process is shown to follow typical ALD characteristics, that is the surface-controlled, self-limiting growth. The effective wavelength range was studied by optical filtering and it appears that the Cu film growth chemistry employs UV light close to 200 nm in wavelength. Despite the inherent anisotropic (directional) character from the UV light, Cu films can be deposited onto structures with moderate aspect ratios. Most importantly, ASD is realized inherently, following the category (3) approach, without any masking, driven by excitation process by photons in the substrate material. Photo-ALD driven by the substrate-photon interactions to our knowledge has not been reported previously. The process resembles photocatalysis and yields pure and low-resistivity copper films on Ta_2O_5. At the same time, the process enables highly selective ASD of copper at high spatial resolution on Ta_2O_5 and extends to facet-selective deposition of copper on anatase TiO_2. Even if the material system is still limited, the unprecedented selectivity in metal film deposition on oxide materials is highly promising and has potential in many applications, such as metallization in microelectronics.

2. Results and Discussion

Process characteristics of Cu Photo-ALD were studied on ALD Ta_2O_5 films deposited on silicon because in the preliminary experiments the process was found to be highly selective for the growth on Ta_2O_5. The films were deposited by repeating a sequence of $Cu(dmap)_2$ – purge – UV–vis light flashes. A single light flash has an energy of about 200 J, duration of a few hundred microseconds and they are repeated with a 5 Hz frequency. Self-limiting nature of the Cu film growth was demonstrated at 150 °C by studying the amount of copper deposited as a function of number of flashes (**Figure 1**). The normalized film thicknesses were calculated from energy-dispersive X-ray spectroscopy (EDS) results as explained in Experimental Section. Since the Photo-ALD Cu films have high roughness, the normalized thicknesses do not represent the actual physical thicknesses of the Cu films but correlate well with the total amount of Cu deposited. It is clear from the plot in Figure 1 that the deposition reaches saturation at around 20 flashes. 1000 Photo-ALD cycles were used for the experiment. Saturation of the Cu precursor reactions was verified with an experiment with two Cu precursor pulses, which produced a Cu film of the same thickness as obtained with one Cu precursor pulse. The growth rate is low, around 0.1 Å $cycle^{-1}$. The same copper precursor was used earlier in thermal ALD by Väyrynen et al.,[20] employing *tert*-butylhydrazine as a reducing reactant. Also, low growth rates of 0.1–0.2 Å $cycle^{-1}$ were measured. It was also observed that the growth rate slowed down after reaching a full coverage of the substrate. $Cu(dmap)_2$ has been employed as a precursor also in other ALD processes of copper metal[21–22] as well as of copper(I) oxide,[23] copper(II) oxide,[24] and hybrid copper-organic material.[25]

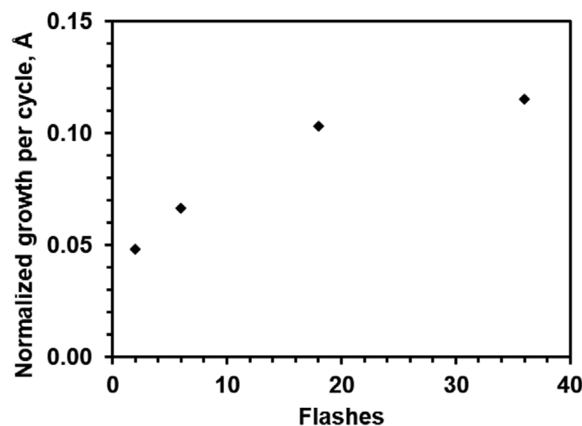

Figure 1. Normalized Cu growth per cycle as a function of UV–Vis flashes (1000 Photo-ALD cycles) per one Photo-ALD cycle.

The Cu Photo-ALD process exhibits a linear relationship between the number of deposition cycles and nominal film thickness calculated from the EDS data (**Figure 2**). Physical thicknesses of the Photo-ALD Cu film were estimated from SEM images of sample cross-sections. They do not follow the same linear function as the nominal thicknesses: after 1000 and 5000 Photo-ALD cycles the films are about 40 and 60 nm thick, respectively. Evaluation of the physical film thickness is, however, challenging because the films are rough. The reason behind the significant difference between the physical thicknesses and the nominal thicknesses in Figure 2 becomes clear from the top-view SEM images in **Figure 3**. The Cu deposits are granular at the beginning of the growth and there are voids between the granules. As the Photo-ALD proceeds further, the

 © 2021 The Authors. Advanced Materials Interfaces published by Wiley-VCH GmbH

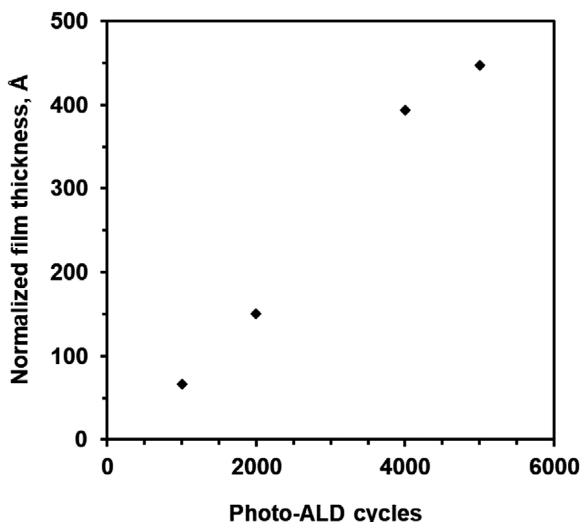

Figure 2. Deposited Cu film thickness as a function of Photo-ALD cycle count (6 flashes per Photo-ALD cycle).

voids fill whereas the physical thickness increases only to a lesser extent. The morphology of the Cu films resembles those deposited by thermal ALD from the same Cu precursor, though there the film closure occurred already after 1000 cycles at a thickness of about 20 nm.[20] Regarding the present study, the development of morphology most likely sustains the Photo-ALD process and allows deposition of thicker films: when the film is not continuous, light can reach the substrate through the voids. If the film was continuous, light would be reflected or absorbed, and Photo-ALD of Cu would be terminated. Therefore, if the agglomeration could be slowed down, one should be able to develop a process that terminates to the thickness where a full coverage is reached. Furthermore, the better the agglomeration would be restricted, the lower this thickness would be.

There is an increase in Cu Photo-ALD growth per cycle as a function of deposition temperature. With 40-UV flash Photo-ALD process, the Cu growths per cycle were 0.01, 0.04, and 0.1 Å at 110, 130, and 150 °C deposition temperatures, similar to the reported findings with the analogous thermal process.[20] In conclusion, our process appears to show all the traditional ALD characteristics.

Compositional analysis by time-of-flight elastic recoil detection analysis (TOF-ERDA) showed that the films were pure from impurities. This is noteworthy, considering that the growth process does not involve reductant or any other reactant, but relies solely on photolytic reactions of the adsorbed Cu precursor molecules. The elemental depth profiles are presented in **Figure 4**. In the profile, the interfaces between Cu and Ta_2O_5 films, and on the other hand between Ta_2O_5 film and Si substrate are not sharp, and the depth resolution is thus decreased. This effect is mostly due to the high roughness of the Cu film: the ions in the ERD primary beam travel through different Cu layer thicknesses, and the same applies to the recoils generated from the Ta_2O_5 film and Si substrate. This, together with method-related effects like multiple scattering, straggling and system resolution, causes rounded depth profiles

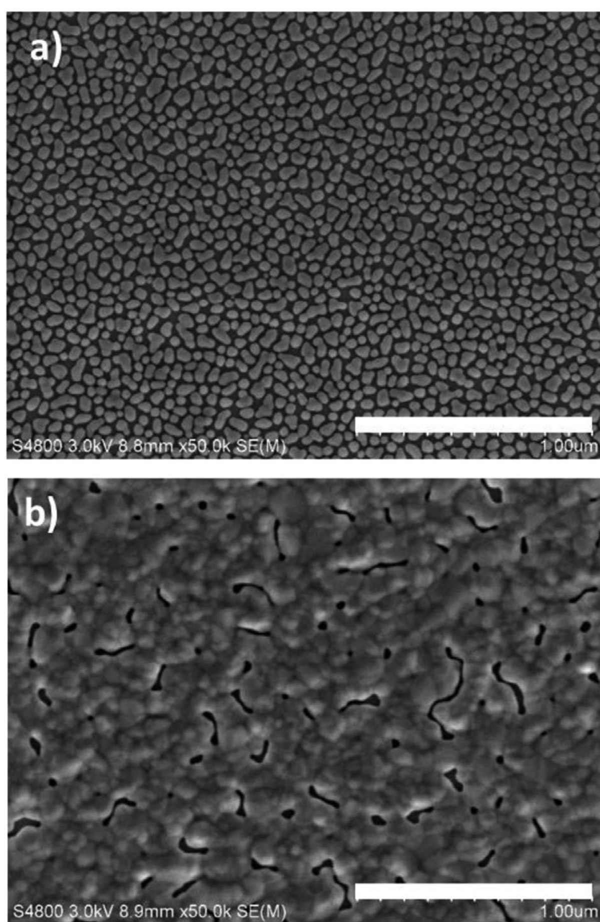

Figure 3. Top-view micrographs on Photo-ALD Cu films, a) 1000 cycles, b) 5000 cycles. Scale bars 1.0 µm, 18 UV flashes per Photo-ALD cycle.

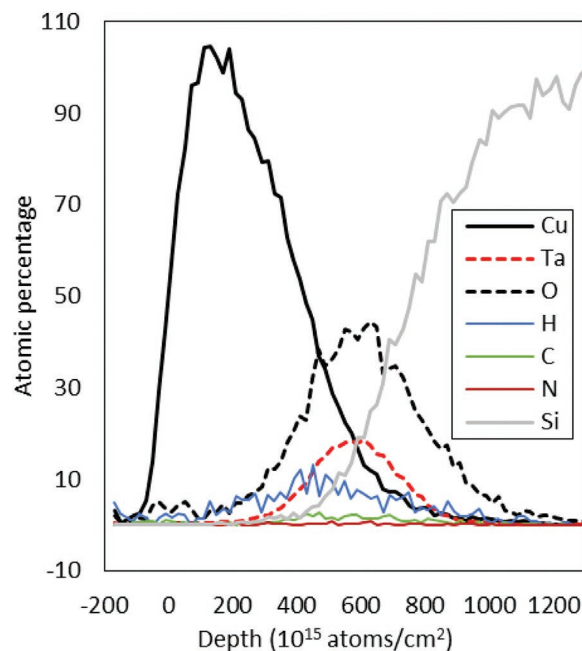

Figure 4. Elemental TOF-ERDA depth profiles of Photo-ALD Cu (5000 Photo-ALD cycles) deposited on ALD-Ta_2O_5 on Si.

© 2021 The Authors. Advanced Materials Interfaces published by Wiley-VCH GmbH

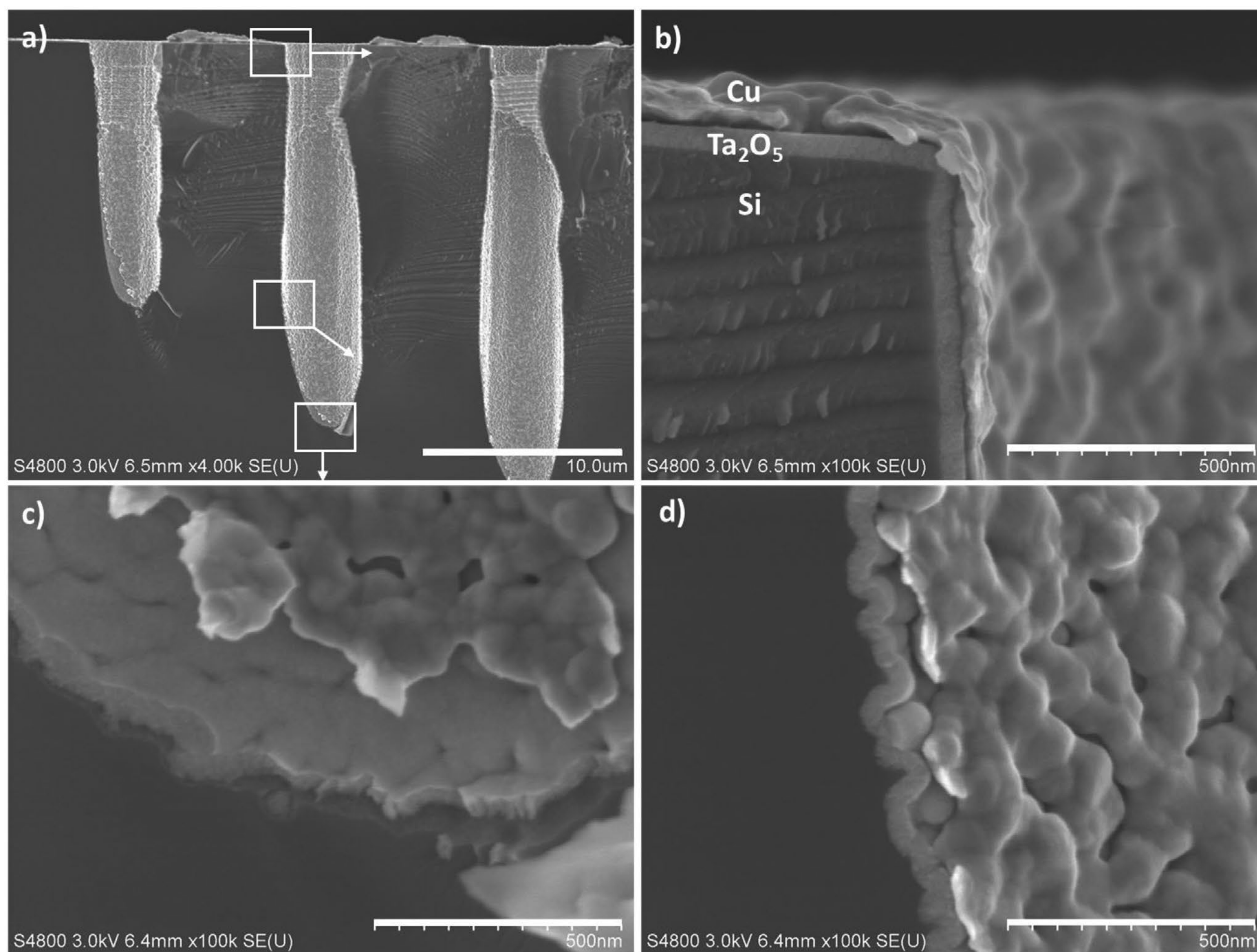

Figure 5. Cross-section micrographs of Photo-ALD Cu (5000 cycles) on pores on ALD-Ta_2O_5-coated silicon. a) Overview, and close-ups b) on top, c) midway, d) on bottom where Cu has partially peeled off during sample preparation. Scale bar 10 µm in (a), 500 nm in others.

as seen in Figure 4. Fully quantitative elemental analysis is difficult to execute for the same reason, but from the TOF-ERDA the impurity contents in the Cu film in *atomic-%±error* were: H < 2.24 ± 0.20; C < 0.20 ± 0.10; O < 2.60 ± 0.15. The film was 95.0 ± 0.6% Cu. Oxygen is slightly enriched in the top part of the film. Most likely this is a result of Cu oxidation due to ambient conditions between the deposition and TOF-ERDA measurement. Similar surface oxidation was observed with Cu films deposited by thermal ALD.[20] Overall, the main impurities in the Photo-ALD Cu films are hydrogen and oxygen, as in the thermal ALD Cu films. Another potential source for the contaminants is residues from the precursors ligands. With Photo-ALD the total impurity content is at a few percent at its maximum, whereas with thermal ALD there were less than a percent of impurities. Both methods can be concluded to produce pure films. Potentially, elongating the time or changing the wavelength of UV exposure could produce even purer films with Photo-ALD.

Features in microelectronic devices are demanding not only by their size but often also by their shape, that is, they are constructed as high aspect ratio pores, trenches, fins or pillars, or as complex nanostructures. As demonstrated also in our previous paper on Photo-ALD of oxides,[12] Photo-ALD has an inherent anisotropic character because photons are employed in the deposition process. Thus, on substrate areas where the surface is perpendicular to the photon flux, the photon dose per unit area is the highest, whereas on tilted surfaces it is smaller. Exposure per unit area follows a cosine function of the angle between the photon flux and surface plane. The anisotropic character is seen here as well. **Figure 5** shows a cross-section of Photo-ALD Cu deposited with 5000 cycles on ALD-Ta_2O_5 on a porous silicon substrate. The film is thicker on the top of the structure, but the film is still continuous all the way to the bottom of the pore, and the film thickness is uniform on walls of the pore. This finding furthermore supports the conclusion that the photolytic process behind the Cu growth is efficient and capable of depositing pure Cu films on moderate-to-high aspect ratio structures. Reflection and scattering of light from the surface are one factor improving the conformality. The most demanding trenches would obviously not be accessible with this process. The directional feature can be, on the other hand, benefitted in certain devices and process designs.

Analogously to our earlier study on Photo-ALD of oxides, we used 1-mm thick slides of soda lime glass and quartz as

© 2021 The Authors. Advanced Materials Interfaces published by Wiley-VCH GmbH

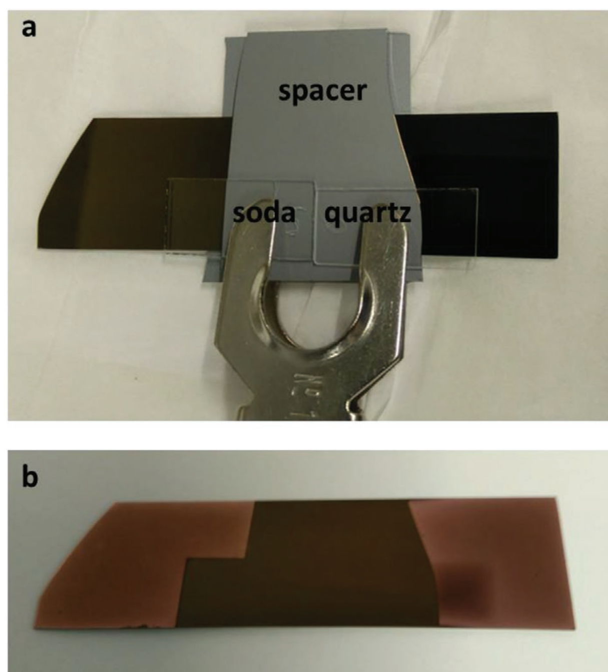

Figure 6. Optical filtering experiment; a) the setup with spacer supporting soda lime glass and quartz optical filters 1 mm above the substrate; b) the resulting Cu film.

optical filters to control the wavelengths of the light reaching the substrate. The glass slides were fixed with a spacer and a clamp 1 mm above the substrate (**Figure 6**a). This setup allows precursors to flow under the glass slides and adsorb onto the substrate surface. The emission spectrum of the xenon lamp ranges from 190 to 800 nm and above, having peak intensity around 400–500 nm. The optical window of the Photo-ALD reactor is transparent down to 190 nm in wavelength. Transmissions of quartz and soda lime glasses at 300 nm wavelength are 90% and 50%, respectively, whereas their transmissions at 200 nm are 70% and 0%, respectively. At longer wavelengths, both glasses are transparent within the light source emission range. As a result of the optical filtering, Photo-ALD is completely blocked by the soda lime glass, whereas under the quartz copper is deposited though it is visually thinner than without any optical filtering (Figure 6b).

Two conclusions can be drawn from these findings considering the transmission of the optical filters and their effect on Photo-ALD. 1) Photo-ALD is driven by UV light and thus electronic excitations are an essential part of the chemical reactions depositing copper in the present process. 2) The effective range for the Cu Photo-ALD process must lie at the short-wavelength end of the current light source, closer to 200 than 300 nm. Effective range may extend to shorter wavelengths, but these are not accessible with our current light source.

Highly selective copper deposition was demonstrated by Photo-ALD on substrates with patterned Ta_2O_5. First, a linear nanopattern was prepared by depositing a nanolaminate of Ta_2O_5 and Al_2O_3 films on silicon by ALD and then cleaving the sample to expose the cross-section of the nanolaminate. Hard but brittle single-crystalline silicon and amorphous oxide

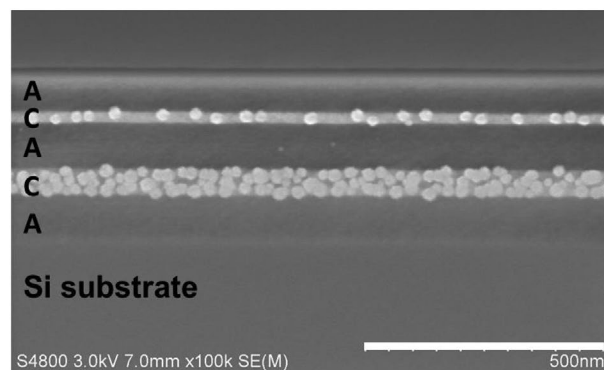

Figure 7. Demonstrator for ASD on Ta_2O_5 lines formed by exposing a cross-section of an Al_2O_3/Ta_2O_5 nanolaminate on Si: 1000 cycles of Photo-ALD deposits Cu only on Ta_2O_5 (C) leaving Al_2O_3 (A) and Si clean. Scale bar 500 nm.

thin film materials allow controlled cleavage producing sharp interfaces. This robust approach enables fabricating well-defined patterns where the linewidths are determined by the layer thicknesses in the nanolaminate. Such a structure was used as a simple demonstrator of ASD (**Figure 7**). Copper was clearly deposited only on the 20 and 50 nm wide Ta_2O_5 lines (C) whereas no copper was deposited on 100 nm wide Al_2O_3 lines (A) and Si substrate.

To deposit Cu patterns in a more integrated way, a combination of focused-ion beam (FIB) and wet etching was used to pattern a substrate. On a coupon of silicon, Ta_2O_5 and Al_2O_3 were deposited by ALD to serve as an active substrate for Cu Photo-ALD and a FIB hard mask, respectively. FIB milling was first used to pattern the Al_2O_3 hard mask, and then the following immersion in 5% aqueous solution of tetramethylammonium hydroxide (TMAH) at 50 °C etched the FIB-patterned Al_2O_3 off and revealed the underlying Ta_2O_5 layer. As a result, a Ta_2O_5 pattern is exposed on the surface. We have used this FIB-milling-wet etch procedure previously also for fabrication of various microstructures in combination with conventional, thermal ALD.[26]

The high selectivity of the Cu deposition is clear also with this approach. Cu deposits solely on Ta_2O_5 exposed by the FIB-wet etching process, leaving Al_2O_3 clean (**Figure 8**). This also very clearly demonstrates the robustness of both the Cu Photo-ALD and the etching processes, as the high selectivity remains regardless of the etching process including exposure to ambient conditions and alkaline solutions. EDS analysis on the Al_2O_3 surface did not show any traces of Cu. Typically in the previously reported approaches to ASD, the selectivity is very sensitive to even minor surface modifications and changes.[2] The present findings obviously point to a deposition mechanism that is different and, most importantly, significantly less sensitive to minor surface changes than the previously reported ASD processes.

To further investigate the selectivity of Cu Photo-ALD, especially at the boundary between Ta_2O_5 and Al_2O_3, the following procedure was applied. First, a two micrometers wide line of Ta_2O_5 was patterned with the FIB-milling-wet etch approach, in the same way as above. Then, 5000 cycles of Cu were deposited with Photo-ALD. Finally, the cross-section of the Cu-Ta_2O_5-Si

 © 2021 The Authors. Advanced Materials Interfaces published by Wiley-VCH GmbH

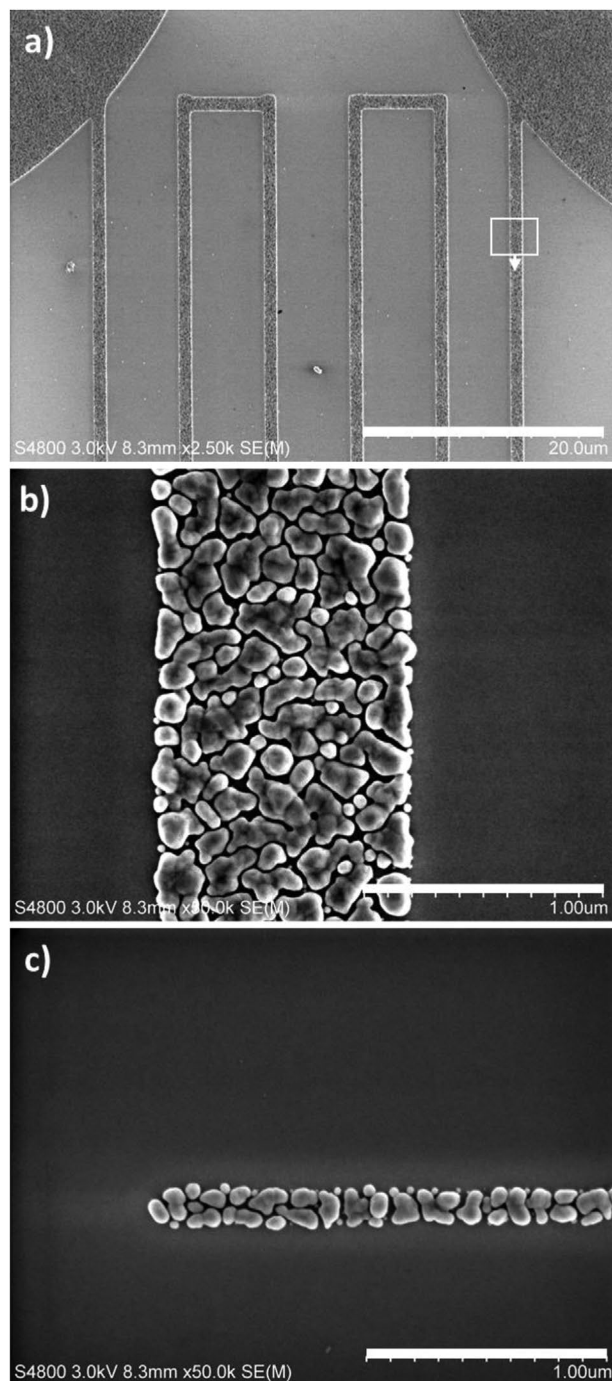

Figure 8. Cu ASD on Ta_2O_5: a) overview of the patterned area, scale bar 20 µm; b) magnification of a Cu line in (a), scale bar 1.0 µm; c) separate 100 nm wide Cu pattern, scale bar 1.0 µm.

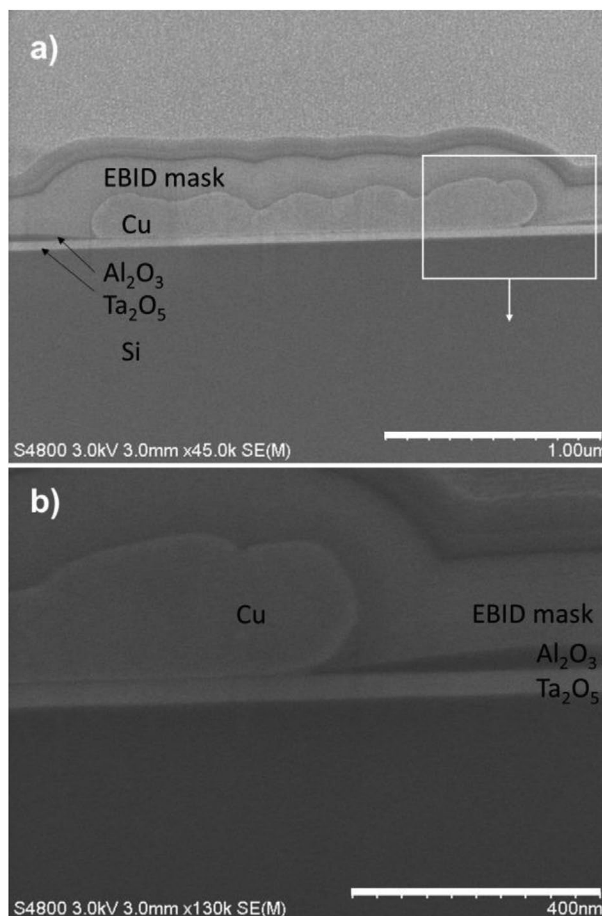

Figure 9. SEM micrograph on the FIB-milled cross-section of Photo-ALD Cu (5000 cycles) on patterned Ta_2O_5: a) overview, b) close-up on the Al_2O_3-Ta_2O_5 boundary.

stack in the resulting sample was FIB-milled and imaged with SEM (**Figure 9**). The Cu deposition occurs again solely on Ta_2O_5 while no Cu deposition takes place on the surrounding Al_2O_3. Furthermore, already a very thin film of Al_2O_3 blocks the Cu Photo-ALD and enables the high selectivity as evident from Figure 9. Let us reflect this finding by following our hypothesis on the mechanism, where photoexcitation in Ta_2O_5 drives the deposition process. The thin Al_2O_3 does allow photons to reach the underlying Ta_2O_5 because it is transparent at the employed wavelengths. However, considering the good insulating properties, most likely Al_2O_3 does not allow the photogenerated electrons and holes to migrate to the surface to participate in the surface reactions for Cu deposition. In any case, the selectivity of Cu deposition on Ta_2O_5 over Al_2O_3 is unprecedented.

By reviewing Figure 9, we can further refine the proposed film growth mechanism. Cu deposited by Photo-ALD is quite thick and there is not much open Ta_2O_5 surface available. Therefore it is more likely that the electrons or holes photogenerated in Ta_2O_5 migrate through the copper onto its surface where the deposition reactions take place, in comparison to a scheme where the surface reaction would take place directly on the Ta_2O_5 surface, and the generated copper would migrate and agglomerate. Metallic nanoparticles are in fact widely applied as cocatalysts in heterogeneous catalysis, where their role is to act as charge traps and promote the separation of the photogenerated charges.[27] Here, the depositing copper may well have a similar effect. Based on reports by Väyrynen et al.[20] and Lee et al.,[21] $Cu(dmap)_2$ adsorbs well on Si and Al_2O_3, and also on polycarbonate, soda lime glass, hydrogen-terminated Si, TiN, and Ru. Thus, it seems unlikely that selective $Cu(dmap)_2$

 © 2021 The Authors. Advanced Materials Interfaces published by Wiley-VCH GmbH

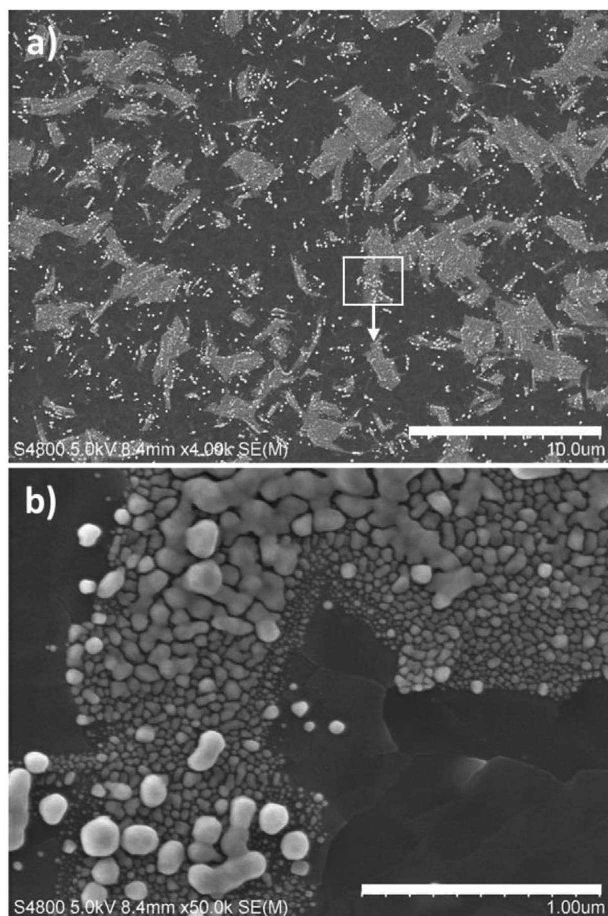

Figure 10. Crystal-facet selective deposition of Cu on TiO_2 by Photo-ALD. a) overview, scale bar 10.0 μm; b) magnification, scale bar 1.0 μm.

adsorption would be the reason for the selective Cu deposition, but the photon-substrate interactions and the reactions following from those.

When Cu Photo-ALD was conducted on polycrystalline ALD anatase TiO_2 film, it was found that Cu appears to deposit facet-selectively. From the top-view SEM (**Figure 10**), Cu clearly deposits only onto some of the crystallites of TiO_2 while some of them remain clean, having no Cu deposited. There are also clear boundaries between the growth and the non-growth areas of Cu, which also appear to align with the TiO_2 grain boundaries. With the methods accessible to us, however, it is not possible to analyze the orientation of the individual TiO_2 crystallites to study which are the crystallites and their exposed facets preferred for Cu Photo-ALD and which are not.

Our present findings about the highly selective and robust Cu deposition suggest that the Photo-ALD of Cu is related to photocatalysis, that is, photons excite the substrate rather than the adsorbed precursor. Furthermore, it appears that the excitation of the substrate leads to chemical reactions that result in deposition of pure Cu films and complete removal of precursor ligands. For TiO_2, photocatalytic processes are widely studied yet not all the details of the catalytic process steps are fully understood. The bandgap of anatase TiO_2 is around 3.2 eV, which corresponds to 390 nm wavelength. The {001} and {101} are known as the high-energy and low-energy facets of anatase, respectively, deriving from their different Ti coordination. The high-energy {001} facets attract UV-generated holes and are thus favorable for oxidative reactions, and the low-energy {101} facets attract electrons being favorable for reductive reactions.[28] While the details of the surface processes in the present case remain as a topic of a follow-up study, it is very likely that the facet-selective Cu Photo-ALD is governed by these differences.

Also, Ta_2O_5 has been studied for photocatalytic applications.[29–31] Nagaraju et al. reported that Ta_2O_5 nanoparticles, crystalline in the orthorhombic phase, were active in photocatalytic decomposition of methylene blue solution under visible light.[29] Zhu et al. in turn found that nanoparticles of crystalline Ta_2O_5 were photocatalytically active in decomposition of gaseous formaldehyde under illumination of a 254-nm UV lamp.[31] Kumar et al. reported an optical band gap of 3.3–4.4 eV (corresponding to 375–282 nm in wavelengths) for amorphous Ta_2O_5 thin films deposited by DC sputtering.[30] They reported high photocatalytic activity for Ta_2O_5 in decomposition of Rhodamine-B solution, upon illumination with 254-nm UV lamp. The prior reports show that the photocatalytic activity of Ta_2O_5 depends on its optical properties, structure, and preparation conditions, but a complete understanding of the correlations between these is lacking. Also, the optical properties of Ta_2O_5 obviously depend on the preparation conditions and the resulting structure of the material. In relation to the present case, the correlation between the substrate bandgap, selectivity of the process, and the wavelength of the employed light source would be the key in controlling the ASD on various substrates. This is a very challenging task as an intensive light source with emission wavelength tunable across the UV range is required to conduct spectroscopic experiments on deposition by Photo-ALD. The mechanism of the photocatalytic reaction in the Photo-ALD must be of a redox-type since metallic Cu in the film is obtained by reducing Cu(II) in the precursor, but understanding the details would require detailed in situ study of the species on the surface and in the gas phase.

The low resistivity of copper is important for its applications but also indicates its high purity. For Photo-ALD Cu on Ta_2O_5, we measured 1.4 and 0.9 $\Omega\ \square^{-1}$ sheet resistance values for 4000-cycle and 5000-cycle films, respectively. For the latter film, which is 60 nm in thickness, the resistivity is thus $5.7 \times 10^{-6}\ \Omega$ cm. That is very close to the bulk Cu resistivity value of $1.7 \times 10^{-6}\ \Omega$ cm, speaking for a pure material and a robust deposition process.

3. Conclusions

To conclude, we have shown in the present work that Photo-ALD can be employed to deposit high-quality, conductive copper films in a self-aligning manner onto Ta_2O_5 films. The sole precursor of the Photo-ALD process, $Cu(dmap)_2$, first adsorbs onto the surface as in conventional ALD. However, upon the following UV–Vis exposure photolytic reactions remove the precursor ligands from the surface and reduce copper without any additional reactant. The results of our optical filtering study

© 2021 The Authors. Advanced Materials Interfaces published by Wiley-VCH GmbH

evidently indicate that the effective wavelength range for copper Photo-ALD lies in the UV, at around 200 nm and towards shorter wavelengths. Most interestingly, copper Photo-ALD can be deposited selectively onto metal oxides without any surface pre-treatment or masking of the surface area. That indicates that the photolytic reaction mechanism in copper Photo-ALD is related to photocatalysis where the photons excite the underlying substrate material, which then enables reactions in the adsorbed precursor.

The fact that copper can be deposited highly selectively onto Ta_2O_5 and TiO_2 is both interesting in the fundamental context of ASD and highly relevant for the microelectronic applications. It is expected that the selective deposition is not limited to the material combinations reported in the present study. The fundamental excitation process that dictates the ASD is defined by the photon energy, electronic properties of the substrate material, and the employed ALD precursor. Hence, it should be possible to control the growth and non-growth areas by adjusting these variables, provided that the correlations are known, as discussed above. In any case, the present study contributes a new chemical approach to the emerging field of ASD which is highly important from the application point-of-view but very challenging to realize.

4. Experimental Section

$Cu(dmap)_2$, was synthesized in-house using a metathesis reaction between sodium dimethylamino-2-propoxide and $CuCl_2$[32] and by isolating the product directly from the reaction mixture by sublimation. Photo-ALD experiments were done with a modified Picosun R-200 reactor (**Figure 11**) described in detail elsewhere.[12] Photon source was Xenon corporation RC-800 series pulsed xenon discharge light source emitting at a UV–Vis range down to 190 nm in wavelength. According to the lamp manufacturer, the pulse energy was 207 J/pulse. The lamp was pulsed at 5 Hz frequency while the pulse duration was a few hundred microseconds. Copper precursor, $Cu(dmap)_2$, was evaporated at 85 °C from PicoHot source which operates with the principle of carrier gas loading and release to ensure efficient precursor delivery. Thin films of amorphous Al_2O_3, anatase TiO_2, and amorphous Ta_2O_5 deposited on Si by ALD, as well as bare Si with the native oxide, were used as substrates for Photo-ALD. XRD analysis demonstrated the TiO_2 film to be randomly oriented, polycrystalline anatase.

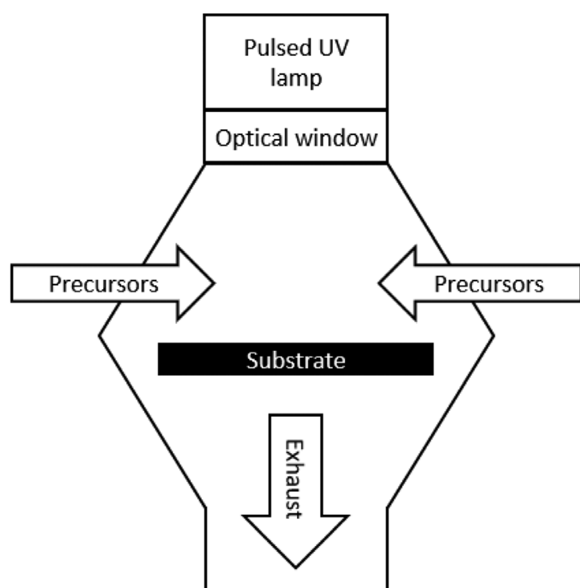

Figure 11. Schematics of the Photo-ALD reactor.

Hitachi S-4800 scanning electron microscope was used for analyzing the film morphology and the physical film thickness from the sample cross-section. The nominal film thickness value was calculated with a GMRFilm software[33] from Cu Lα, Ta Mα, and O Kα k-ratios from EDS data (Oxford INCA 350 energy spectrometer), using bulk densities of 8.96 and, 8.18 g cm^{-3} for Cu and Ta_2O_5, respectively. Cu film sheet resistance was measured by four-point probe (CPS Probe Station by Cascade Microtech) combined with a Keithley 2400 Source Meter. Resistivity of the Cu film was then calculated by multiplying the sheet resistance by the physical film thickness. A FIB-SEM dual beam system (FEI Quanta 3D 200i) was used for surface patterning and preparation of the cross-section sample. Aqueous solution of 5% TMAH was used for the wet etching at a temperature of 50 °C. TOF-ERDA was used for Cu film compositional analysis and elemental depth profiling. Measurement was done with 40 MeV $^{79}Br^{+7}$ beam. The incident beam was at a 16 degrees angle with respect to the sample surface, and the recoil ions were collected at an angle of 24 degrees.

Acknowledgements

Semiconductor Research Corporation (SRC) and Academy of Finland (both Finnish Centre of Excellence in Atomic Layer Deposition (ALDCoE) and a project ALD of Noble Metals and Their Compounds, decision number 309552) are gratefully acknowledged for funding this research. Picosun is thanked for providing the specially modified Photo-ALD reactor for this project.

Conflict of Interest

The authors declare no conflict of interest.

Data Availability Statement

The data that support the findings of this study are available from the corresponding author upon reasonable request.

Keywords

area-selective deposition, atomic layer deposition, copper films, photo-assisted deposition, photocatalysis

Received: January 5, 2021
Revised: February 26, 2021
Published online: May 6, 2021

[1] V. Miikkulainen, M. Leskelä, M. Ritala, R. L. Puurunen, *J. Appl. Phys.* **2013**, *113*, 021301.
[2] A. J. M. Mackus, M. J. M. Merkx, W. M. M. Kessels, *Chem. Mater.* **2019**, *31*, 2.
[3] R. Clark, K. Tapily, K.-H. Yu, V. Hakamata, S. Consiglio, D. O'Meara, C. Wajda, J. Smith, G. Leusink, *APL Mater.* **2018**, *6*, 058203.
[4] X. Jiang, S. F. Bent, *J. Phys. Chem. C* **2009**, *113*, 17613.
[5] E. Färm, M. Kemell, M. Ritala, M. Leskelä, *Chem. Vap. Deposition* **2006**, *12*, 415.
[6] E. Färm, S. Lindroos, M. Ritala, M. Leskelä, *Chem. Mater.* **2012**, *24*, 275.

© 2021 The Authors. Advanced Materials Interfaces published by Wiley-VCH GmbH

[7] A. J. M. Mackus, N. F. W. Thissen, J. J. L. Mulders, P. H. F. Trompenaars, M. A. Verheijen, A. A. Bol, W. M. M. Kessels, *J. Phys. Chem. C* **2013**, *117*, 10788.
[8] B. Kalanyan, P. C. Lemaire, S. E. Anatasov, M. J. Ritz, G. N. Parsons, *Chem. Mater.* **2016**, *28*, 117.
[9] P. C. Lemaire, M. King, G. N. Parsons, *J. Chem. Phys.* **2017**, *146*, 052811.
[10] Z. Yang, N. Li, X. Wang, Z. Wang, Z. Wang, *Electrochem. Solid-State Lett.* **2010**, *13*, D47.
[11] H. R. Radamson, K. Mohammadreza, *J. Mater. Sci.: Mater. Electron.* **2015**, *26*, 4584.
[12] V. Miikkulainen, K. Väyrynen, K. Mizohata, J. Räisänen, M. Vehkamäki, M. Ritala, *J. Vac. Sci. Technol., A* **2019**, *37*, 060911.
[13] A. Doi, Y. Aoyagi, S. Namba, *Appl. Phys. Lett.* **1986**, *49*, 785.
[14] Q. Chen, P. D. Dapkus, *Thin Solid Films* **1993**, *225*, 115.
[15] K. Saito, Y. Watanabe, K. Takahashi, T. Matsuzawa, B. Sang, M. Konagai, *Sol. Energy Mater. Sol. Cells* **1997**, *49*, 187.
[16] J.-C. Kwak, Y.-H. Lee, B.-H. Choi, *Appl. Surf. Sci.* **2004**, *230*, 249.
[17] J. Olander, L. M. Ottosson, P. Heszler, J.-O. Carlsson, K. M. E. Larsson, *Chem. Vap. Deposition* **2005**, *11*, 330.
[18] B. H. Lee, S. Cho, J. K. Hwang, S. H. Kim, M. M. Sung, *Thin Solid Films* **2010**, *518*, 6432.
[19] P. R. Chalker, P. A. Marshall, K. Dawson, I. F. Brunell, C. J. Sutcliffe, R. J. Potter, *AIP Adv.* **2015**, *5*, 017115.
[20] K. Väyrynen, K. Mizohata, J. Räisänen, D. Peeters, A. Devi, M. Ritala, M. Leskelä, *Chem. Mater.* **2017**, *29*, 6502.
[21] B. H. Lee, J. K. Hwang, J. W. Nam, S. U. Lee, J. T. Kim, S.-M. Koo, A. Baunemann, R. A. Fischer, M. M. Sung, *Angew. Chem., Int. Ed.* **2009**, *48*, 4536.
[22] Y. Maimati, S. D. Elliott, *Chem. Mater.* **2016**, *28*, 6282.
[23] J. R. Avila, A. W. Peters, Z. Li, M. A. Ortuño, A. B. F. Martinson, C. J. Cramer, J. T. Hupp, O. K. Farha, *Dalton Trans.* **2017**, *46*, 5790.
[24] T. Iivonen, J. Hämäläinen, B. Marchand, K. Mizohata, M. Mattinen, G. Popov, J. Kim, R. A. Fischer, M. Leskelä, *J. Vac. Sci. Technol., A* **2016**, *34*, 01A109.
[25] D. J. Hagen, L. Mai, A. Devi, J. Sainio, M. Karppinen, *Dalton Trans.* **2018**, *47*, 15791.
[26] Z. Han, E. Salmi, M. Vehkamäki, M. Leskelä, M. Ritala, *Nanotechnology* **2018**, *29*, 055301.
[27] Y. Yang, D. Wang, H. Han, C. Li, *Acc. Chem. Res.* **2013**, *46*, 1900.
[28] N. Roy, Y. Sohn, D. Pradhan, *ACS Nano* **2013**, *7*, 2532.
[29] G. Nagaraju, K. Karthik, M. Shashank, *Microchem. J.* **2019**, *147*, 749.
[30] K. Jagadeesh Kumar, N. Ravi Chandra Raju, A. Subrahmanyam, *Surf. Coat. Technol.* **2011**, *205*, S26.
[31] Y. Zhu, F. Yu, Y. Man, Q. Tian, Y. He, N. Wu, *J. Solid State Chem.* **2005**, *178*, 224.
[32] T. H. Baum, G. Bhandari, C. Xu, *US 6822107*, **2004**.
[33] R. A. Waldo, *Microbeam Anal.* **1988**, *23*, 310.

© 2021 The Authors. Advanced Materials Interfaces published by Wiley-VCH GmbH